Effect of DBD plasma actuation on structures in a plane mixing layer

Yadala, Srikar; Benard, Nicolas; Kotsonis, Marios; Moreau, Eric

DOI
10.2514/6.2020-2152

Publication date
2020

Document Version
Final published version

Published in
AIAA Scitech 2020 Forum

AIAA SciTech Forum
6-10 January 2020, Orlando, FL
AIAA Scitech 2020 Forum

10.2514/6.2020-2152

Effect of DBD plasma actuation on structures in a plane mixing layer

Srikar Yadala*[1,2], Nicolas Benard†[1], Marios Kotsonis‡[2], and Eric Moreau§[1]
[1]*Institut PPRIME, Université de Poitiers (CNRS UPR 3346, ISAE-ENSMA), Boulevard Marie et Pierre Curie, BP 30179, 86962 Futuroscope, France*
[2]*AWEP Department, Section of Aerodynamics, Delft University of Technology, Kluyverweg 1, 2629HS Delft, The Netherlands*

The influence of spanwise-uniform (linear) forcing applied by a dielectric barrier discharge (DBD) plasma actuator on the growth of a plane mixing layer and the dynamics of large-scale spanwise vortices within, are investigated experimentally. Quantitative spatio-temporal measurement of the flow field is acquired using high-speed planar particle image velocimetry. The DBD actuator is used to impart perturbations into the mixing layer to force the fundamental Kelvin-Helmholtz instability and its first sub-harmonic. Forcing the fundamental instability resulted in the inhibition of vortex pairing due to the attenuation of sub-harmonic instabilities. Correspondingly, the growth of the mixing layer is halted initially. With sub-harmonic instability forcing, two vortices interact with each other and merge together. This results in a higher growth rate compared to the unforced mixing layer at the streamwise location of this vortex interaction. Eventually, the growth rate of the forced mixing layer becomes similar to that of the unforced mixing layer. These results demonstrate the influence of the applied forcing on the growth of the turbulent mixing layer and the dynamics of the coherent vortical structures within.

Nomenclature

Symbols

x	Axis along the streamwise direction
y	Axis orthogonal to the streamwise direction
z	Axis parallel to the splitter-plate trailing edge
uvw	Velocity components along the xyz axes
U_1	Streamwise velocity of low-velocity stream
U_2	Streamwise velocity of high-velocity stream
ΔU	Velocity difference between two streams ($= U_2 - U_1$)
$\overline{U}$	Average velocity of the two streams ($= (U_2 + U_1)/2$)
r	Velocity ratio ($= U_1/U_2$)
λ	Velocity ratio ($= \Delta U/(2\overline{U})$)
$y_{0.5}$	y-coordinate where $\overline{u} = U_1 + 0.5 \cdot \Delta U$
δ_w	Vorticity thickness
δ_0	Vorticity thickness at the onset of mixing layer
c	Growth rate fitting parameter
R_{xy}	Reynolds shear stress ($= -\overline{u'v'}$)
f	Frequency
f_0	Frequency of the fundamental Kelvin-Helmholtz instability
Φ^γ	Power spectral density of some quantity γ
ϕ	Phase along burst modulation cycle
V_{ac}	AC voltage amplitude
f_{ac}	AC carrier frequency
f_b	Burst modulation frequency
$\overline{\dots}$	Time-average
$\dots'$	Fluctuating fields
$\dots_N$	Normalized quantities

*PhD candidate, srikar.yadala.venkata@univ-poitiers.fr
†Associate Professor, nicolas.benard@univ-poitiers.fr, AIAA senior member
‡Associate Professor, m.kotsonis@tudelft.nl
§Professor, eric.moreau@univ-poitiers.fr

I. Introduction

The study of flow characteristics in a turbulent mixing layer is very significant for practical aerodynamics. Such a flow arrangement governs the rate of mixing in combustion chambers, flow in jets and wakes among others. It is also a major source of broadband noise associated with jet propulsion. Furthermore, flow over modern aircraft wings is dominated by complex interactions between free-shear flows. A plane mixing layer is the simplest representation of a free-shear flow that attains a self-similar state [1, 2]. Thus, understanding and devising methods to control the structures and growth of a plane mixing layer is instrumental towards improving the performance of many aero-thermo-dynamic systems.

The interaction of two parallel streams with different freestream velocity gives rise, at the trailing-edge of a splitter plate, to a plane mixing layer which is characterised by large-scale, spanwise (coherent) vortices [1]. The mixing layer flow field is unstable to the perturbations arising from the inviscid Kelvin-Helmholtz (KH) instability mechanism. This leads to an exponential growth of two-dimensional waves (primary instability) downstream of the splitter plate, ultimately resulting in their roll-up into discrete spanwise vortices [3]. The amalgamation or pairing of subsequent spanwise vortices, or vortex pairing, has a significant influence on the growth of the mixing layer [2, 4]. Studies have shown [5–7] that sub-harmonic frequencies of the most-amplified KH instability forming immediately downstream of the splitter plate, act as catalyst to the vortex pairing process and hence influence the growth of the mixing layer.

Dielectric barrier discharge (DBD) plasma actuators work on the principle of air ionisation. The authority of these actuators as a flow control device can be attributed to a volume distributed Coulombian or electro-fluid-dynamic (EFD) body force. This is a result of air ionisation and collision of these ions with neutral air particles in the vicinity, when supplied with an alterating current (AC) signal. A thorough review on the basic principles and working mechanism of these actuators can be found in [8]. These actuators have gathered considerable attention as active flow control devices in recent years. This is mainly due to their simple design, high frequency response, low power consumption and their ability to apply the necessary forcing without the use of any mechanical or pneumatic means. DBD plasma actuators have found many successful boundary layer flow control applications for instability control (see for example [9, 10]) and turbulent drag reduction [11].

In contrast to laminar/transitional and wall-bounded flow configurations, previous work on application of DBD plasma actuators in turbulent mixing layers is limited [12, 13]. In the current research, the effect of spanwise-uniform (linear) EFD forcing exerted by a DBD plasma actuator on the spanwise vortices in a mixing layer and the subsequent pairing process is investigated experimentally. This article is organised as follows: the experimental set-up is introduced in section II. Results pertaining to the characterisation of the unforced mixing layer is presented in section III and the influence of the applied EFD forcing on the mixing layer is discussed in section IV. The conclusions drawn from this study are in section V.

II. Experimental set-up

A. Wind-tunnel

The experiments were carried out in a closed-loop wind-tunnel, specially modified to accommodate mixing layer studies. The dimensions of the test-section are 30 cm × 30 cm × 1.2 m in height, width and length respectively. As illustrated in figure 1, a 15 mm thick aluminium (splitter) plate extended from the entrance of the settling chamber, just after the honeycomb, through the convergent and until the entrance of the test section, splitting this section of the wind-tunnel into two equal halves along the vertical direction. This lead to the generation of two parallel flow streams. In order to realize a difference in the velocity between the two streams, a combination of foams and a perforated plate was installed just upstream of the convergent, in the bottom stream, to reduce its velocity. A set of four metallic grids was installed downstream of the perforated plate to reduce the level of freestream turbulence in this stream.

The base-flow configuration selected for this study and used in all cases reported here, was a two-dimensional plane mixing layer formed between two streams of air with freestream velocities maintained at $U_1 = 5$ m s^{-1} (bottom) and $U_2 = 10$ m s^{-1} (top). This resulted in a velocity ratio of $r = U_1/U_2 = 0.5$. Two other velocity parameters are utilized in this article which are introduced here. The first is the velocity difference between the two streams $\Delta U = U_2 - U_1 = 5$ m s^{-1}. The second parameter is the average of the two free stream velocities $\overline{U} = (U_2 + U_1)/2 = 7.5$ m s^{-1} which is expected to be the convection speed of the spanwise vortices in the ensuing mixing layer [14]. Turbulence intensity was measured in both streams with a single hot-wire sensor. The turbulence intensity in the low and high-velocity streams was about $\overline{Tu}/U_{1,2} \approx 0.2\%$. It is worth noting here that the initial boundary layers on both the high- and low-velocity

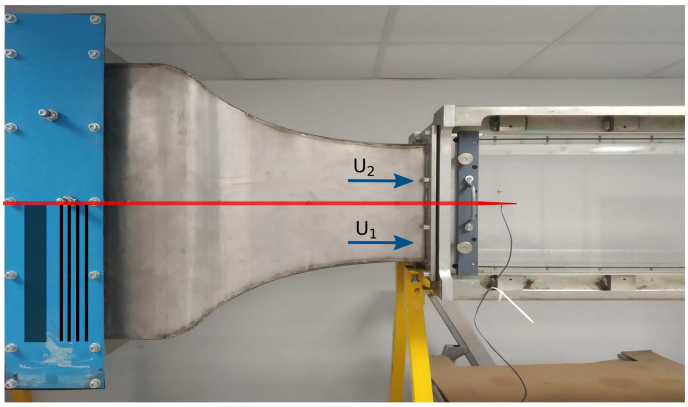

Fig. 1 Wind-tunnel set-up. The location of the foams and perforated plate to achieve a velocity reduction in the bottom stream is represented by a dark rectangle and the four vertical lines represent the metallic grids. The splitter plate is represented in red.

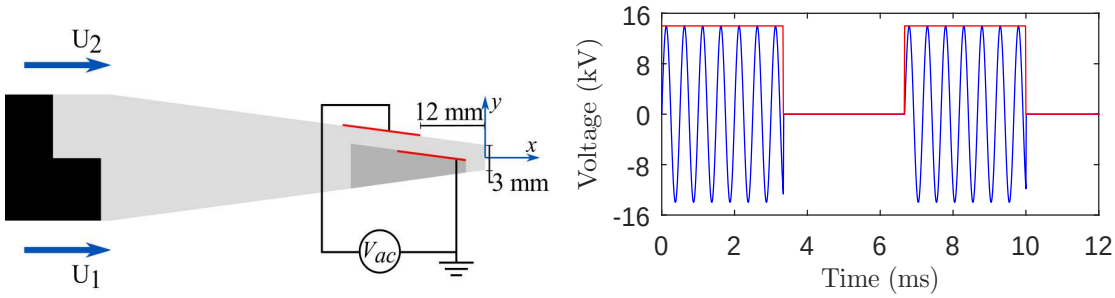

Fig. 2 (a) Splitter-plate edge design (not to scale). The aluminium plate (black), the PMMA splitter-plate edge (light gray), electrodes of the DBD plasma actuator (red lines), the epoxy resin encapsulating the grounded electrode (dark gray) are shown. The coordinate system used in this study is also depicted. (b) Sample input waveform (blue) and square-wave burst modulation (red). $V_{ac} = 14$ **kV,** $f_{ac} = 2$ **kHz,** $f_b = 150$ **Hz.**

sides are not tripped.

The coordinate system used in this study is represented by (x, y, z) where x is along the freestream direction, y is perpendicular to the plane of the mixing layer and z is along the span. The corresponding velocity components are represented by u v and w respectively. The geometrical origin of the mixing layer is fixed at the trailing-edge of the splitter plate (see figure 2a), with $z = 0$ being at the centre of the splitter plate along the span (15 cm from both walls).

B. DBD plasma actuator

The end of the aluminium plate mentioned in section II.A (black area in figure 2a) is attached with a PMMA fixture that has a 120 mm long taper of about 3.1° on both the top and bottom sides. This results in a 3 mm thick trailing-edge. The design of this PMMA fixture is presented in figure 2a. The use of PMMA as the material for this fixture is motivated by its additional application as the dielectric for the DBD plasma actuator. In order to realize this, a spanwise incision (from $x = -42$ mm to $x = -2$ mm, dark gray area in figure 2a) was produced on bottom side of the fixture such that 2 mm thick PMMA remains on the top side. This 2 mm thick PMMA served as the dielectric substrate.

The DBD plasma actuator was constructed just before the trailing-edge of the splitter plate, on the PMMA fixture as shown in figure 2a. [12] observed that the DBD actuator has more control authority on the mixing layer when the EFD forcing is applied in the splitter-plate boundary layer generated by the high-velocity stream. Thus, in the current experiment, the air-exposed electrode of the DBD actuator was flush-mounted on the high-velocity (top) side of the PMMA fixture. The second electrode was installed inside the incision which was then filled with an epoxy resin to encapsulate the second electrode, thus avoiding any unwanted spark generation between the electrodes.

The electrodes of the DBD plasma actuator were uniform strips of aluminium with a non-reflective black coating.

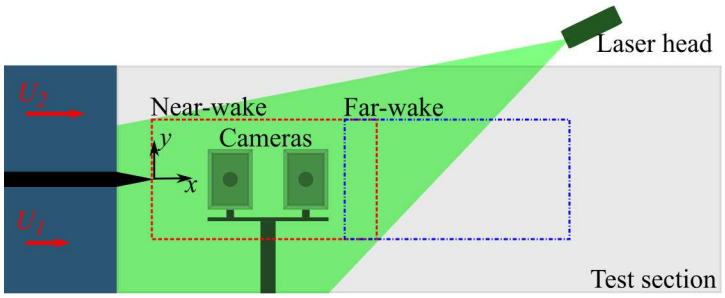

Fig. 3 PIV experimental set-up. The test section, splitter plate, PIV cameras, laser-head and laser sheet are depicted. The freestream velocities and the coordinate system are also shown. The two captured fields: near-wake (dashed red rectangle) and far-wake (dash-dotted blue rectangle) are also presented.

The air-exposed electrode was 50 mm wide while the encapsulated electrode was 15 mm wide. The electrodes were mounted asymmetrically with a relative overlap of 5 mm to ensure consistent plasma generation. This construction resulted in a DBD plasma actuator that exerts a spanwise-uniform forcing along the freestream direction at $x = -12$ mm which is the location of the plasma-generating edge of the air-exposed electrode. The EFD forcing is applied along the streamwise direction as the intention here is to impart fluctuations into the mixing layer flow field in order to amplify certain KH instabilities.

The air-exposed electrode was supplied with the high-voltage AC signal while the encapsulated electrode was grounded. The AC voltage waveform was sinusoidal with amplitude $V_{ac} = 14$ kV adn frequency $f_{ac} = 2$ kHz. Furthermore, a low-frequency (f_b) burst modulation (square waveform) was applied on the input AC waveform. A sample of the resulting input signal is depicted in figure 2b. The actuator was powered using a *Trek 30/20A* (±30 kV, 20 mA) high-voltage amplifier. The amplifier applied a gain of 3 kV/V to the input voltage provided by a *Lecroy WaveStation 3082* function generator.

C. Particle image velocimetry

High-speed planar particle image velocity (PIV) was employed for the characterization of the flow field velocity. The experimental set-up is as shown in figure 3. The inspected plane is along the $x - y$ directions at mid-span ($z = 0$). The flow was seeded with particles of dielectric oil (*Shell Ondina*) injected upstream of the wind-tunnel convergence. A Nd:YAG high speed *Continuum Mesa PIV* laser (18 mJ per pulse) was employed for particle illumination from downstream. The laser head was also placed outside the wind tunnel and the light beam was shaped into a 1 mm thick light sheet. The imaging of the necessary field of view (FOV) was carried out using two *Photron FastCAM SA-Z* cameras featuring a 1024×1024 px^2 CMOS sensor (with 20 μm pixels and 12 bits of digital resolution). Both cameras were installed outside the wind-tunnel test section at about 0.5 m from the measurement plane which they imaged through an optical window. The cameras were equipped with a Nikon Nikkor 50 mm lens operated at $f_\# = 2$. The resulting magnification factor of each camera is $M = 0.12$.

The two cameras were placed adjacent to each other such that their respective FOVs overlap each other by about 26 mm. A calibration plate was employed to stitch the fields captured by the two cameras using *Lavision Davis 8.4.0* suite which resulted in a final FOV of 318×169 mm^2. The plate was 600 mm $\times$ 300 mm in length and height respectively and contained 30×15 black dots (5 mm diameter) separated from each other by 20 mm in both directions. This arrangement (2 cameras and laser) was traversed along the streamwise direction to capture two fields. The first field (near-wake, dashed (red) rectangle in figure 3) spanned from just upstream of the splitter-plate trailing-edge to about $x = 310$ mm while the second field (far-wake, dash-dotted (blue) rectangle in figure 3) spanned from about $x = 285$ mm to $x = 605$ mm. These two fields overlap each other by about 26 mm as well and were stitched together using the same calibration plate with an in-house *MatLab* script. The size of the resulting FOV was 610×169 mm^2.

The laser and the two cameras were synchronized using a *Lavision High Speed Controller* and *Lavision Davis 8.4.0* suite. Furthermore, in order to achieve an acquisition synchronised with the operation of the DBD plasma actuator, the trigger to initiate the PIV acquisition was provided by the same *Lecroy WaveStation 3082* function generator which provided the input signal for the operation of the DBD actuator. The trigger to the PIV system was synchronized with the beginning of a burst modulation cycle ($t = 0$ s in figure 2b). It is worth noting that for all tested cases, the DBD plasma actuator was operational for a few seconds before the start of the PIV acquisition. This was to ensure that the

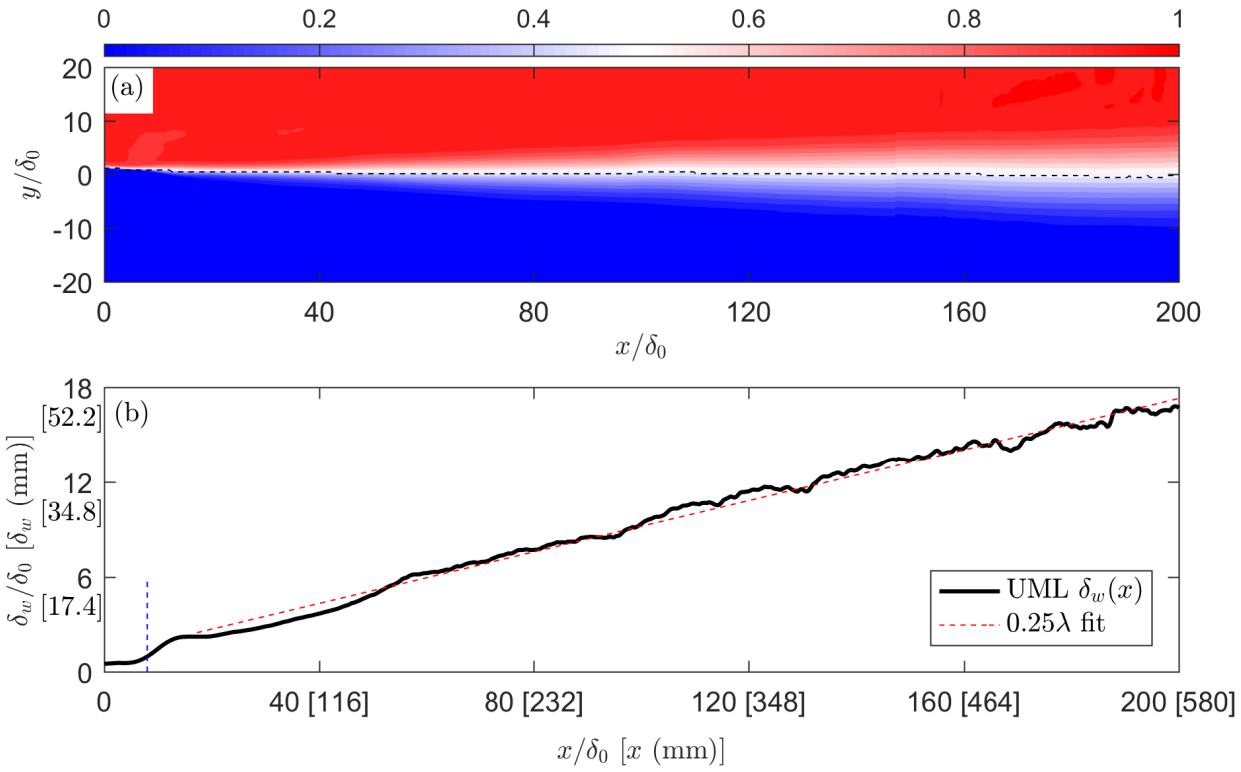

Fig. 4 (a) Time-averaged, normalised u-velocity ($\overline{u}_N$) of the unforced mixing layer. The dashed (black) line in (a) represents $y_{0.5}$. (b) Vorticity thickness along the streamwise direction. Axis values in [] are dimensional (in mm).

mixing layer has reorganised itself according to the applied EFD forcing before the PIV acquisition.

Image acquisition, pre-processing and cross-correlation were performed using the same software package. Cross-correlation was carried out with a final interrogation window of 12×12 px^2 with a relative overlap of 50%. The final vector spacing is 1 mm in both x and y directions. The acquisition rate during all the tested cases was 9.5 kHz in single-frame mode. Thus, the pulse separation between subsequent frames was 105 μs. A sequence of 20000 images were acquired using both the cameras for every tested flow case. The resulting measurement time was 2.1 s per test case.

III. Unforced mixing layer

The baseline flow configuration of the ensuing plane mixing layer is studied here. As mentioned in section II.A, the velocity of the bottom and top flow streams is $U_1 = 5$ m s^{-1} and $U_2 = 10$ m s^{-1} respectively, resulting in a velocity ratio $r = 0.5$. It is good to note that the DBD plasma actuator is mounted on the splitter plate (figure 2a) but not operational while acquiring the PIV fields for the baseline. Thus, this case is henceforth referred to as *unforced mixing layer* (UML).

The normalised, time-averaged u-velocity component ($\overline{u}_N$) is presented in figure 4a. The normalisation of the mean field is performed according to equation 1.

$$\overline{u}_N = \frac{\overline{u} - U_1}{\Delta U} \tag{1}$$

The $\overline{u}_N$ velocity presented in figure 4a contains both the near-wake and far-wake PIV FOVs. The mixing layer developed due to the interaction of the high and low-velocity flow streams downstream of the splitter-plate trailing edge is clearly visible. Also shown in this figure is the location of $y_{0.5}$ which is the y-coordinate where $\overline{u} = U_1 + 0.5 \cdot \Delta U$ (or $\overline{u}_N = 0.5$).

The splitter plate employed for this study has a 3 mm thick trailing edge as discussed in section II.B. This results in a wake effect that manifests as the formation of a recirculation region just downstream of the splitter-plate trailing edge as also observed by [15] who performed direct numerical simulation (DNS) to study the effect of such splitter-plate

trailing edge shape (among others) on the spatial development of the mixing layer. However, it is good to note that the thickness of the current trailing edge is much lower than the case with a similar splitter-plate shape in the DNS study [15]. In the current unforced mixing layer the recirculation region is observed to last until about $x \approx 24$ mm. Beyond this streamwise location, the occurrence of the mixing layer is observed. Hence, the vorticity thickness (δ_w) computed according to equation 2, at $x = 24$ mm being $\delta_0 = 2.9$ mm (vertical dashed blue line in figure 4b) is considered as the reference value and utilized, in what follows, to non-dimensionalise the spatial coordinates. Additionally, the boundary layers on both the high- and low-velocity side were found to be laminar.

$$\delta_w = \frac{\Delta U}{(d\overline{u}/dy)_{max}} \tag{2}$$

The vorticity thickness of the unforced mixing layer along the streamwise direction is presented in figure 4b. Until $x/\delta_0 = 8$ ($x = 24$ mm) no growth is observed due to the occurrence of the recirculation region. A sudden increase in the vorticity thickness is observed just downstream of this location which is the signature of the roll-up of the first vortices and onset of the mixing layer. This is followed by a linear growth from $x/\delta_0 \approx 20$ which can be attributed to vortex pairing occurring stochastically in space and time. This linear growth observed for a major part of the current mixing layer, is in line with previous observations [2, 5, 16]. It is also noteworthy that the growth pattern of the current mixing layer resembles that of the mixing layer ensuing from a thin trailing edge in the numerical work of [15]. The spreading rate of the mixing layer can be approximated by the Abramovich-Sabin rule [17, 18] given by $d\delta_w/dx = c \cdot \lambda$ where the velocity ratio $\lambda = \Delta U/(2\overline{U}) = 0.33$. Constant c is the fitting parameter. In the linear growth region of the current unforced mixing layer, the spreading rate is $d\delta_w/dx = 0.25 \cdot \lambda$ (dashed red line in figure 4b). The value of the fitting parameter $c = 0.25$ is lower than that reported by [15] ($c = 0.34$) for their mixing layer ensuing from a thin trailing edge. This is attributed to the fact that, while performing DNS, the flow is generated with a hyperbolic tangent profile which did not account for the splitter-plate wake. However, the fitting parameter of the current mixing layer is similar to that observed in the experiments of [16].

Profiles of the Reynold's shear stress (R_{xy}) non-dimensionalised with $(\Delta U)^2$, at different streamwise locations are presented in figure 5a. It is worth noting that the y-coordinate in this plot is non-dimensionalised with the local vorticity thickness ($\delta_w(x)$). Similar to the observations of [19] with a thick splitter-plate trailing edge, in the region where the wake effect is significant, the profiles of the Reynold's stress contain two extrema. The high-velocity side has a positive extremum while the low-velocity side contains a comparitively smaller negative extremum as seen in the profile at $x/\delta_0 = 10$ (more pronounced further upstream). The negative extremum decreases along the stream and eventually disappears indicating the decrease in the influence of the splitter-plate wake. Once the wake effect is overcome by the mixing layer, the Reynold's stress profiles have a classical bell-shape with just one extremum within the mixing layer as seen in previous works [2, 16, 19, 20].

In the current unforced mixing layer the mean velocity profiles collapse onto a hyperbolic tangent ($tanh$) profile after $x/\delta_0 = 25$. Furthermore, the mixing layer has a linear growth downstream of this location (figure 4b) which suggests that, with respect to the mean flow, the current mixing layer achieves self-similarity at $x/\delta_0 = 25$. However, as observed in previous works [20, 21], the turbulent properties become self-similar further downstream. The Reynold's shear stress profiles collapse on to each other after $x/\delta_0 \approx 80$. The maximum Reynolds shear stress here is $[R_{xy}/(\Delta U)^2]_{max} = 0.015$ which is comparable to the value observed by [2] (0.013) in their experimental investigation. Downstream of $x/\delta_0 \approx 130$, the maximum Reynolds shear stress in the mixing layer is observed to decrease as seen in the profiles at $x/\delta_0 = 160$ and 200. This is similar to the observations of [20] in their experimental investigation of mixing layers generated by two untripped boundary layer as is the case in the present study.

As mentioned previously, the characteristic spanwise vortices that exist in a mixing layer arise from the inviscid KH instability [1, 3]. The subsequent amalgamation of these vortices depend on the presence and strength of sub-harmonic instability waves of the most-amplified KH instability forming immediately downstream of the splitter plate [5–7]. Thus, knowing the frequency (or wavelength) of the two-dimensional waves forming initially is absolutely necessary.

Time-series of the fluctuations of the transversal velocity component (v') sampled along the $y_{0.5}$ line in the unforced mixing layer (dashed (black) line in figure 4a) are analysed in the Fourier domain. The power spectra are computed using the Welch's method with a final frequency resolution of $\Delta f = 5$ Hz. The spectra are normalized by equation 3 (in agreement with Parseval's theorem),

$$\Phi_N^{v'} \cdot \Delta f = (\Phi^{v'} \cdot \Delta f) \frac{\frac{1}{ES-1} \sum_t (v')^2}{\sum_f (\Phi^{v'} \cdot \Delta f)} \tag{3}$$

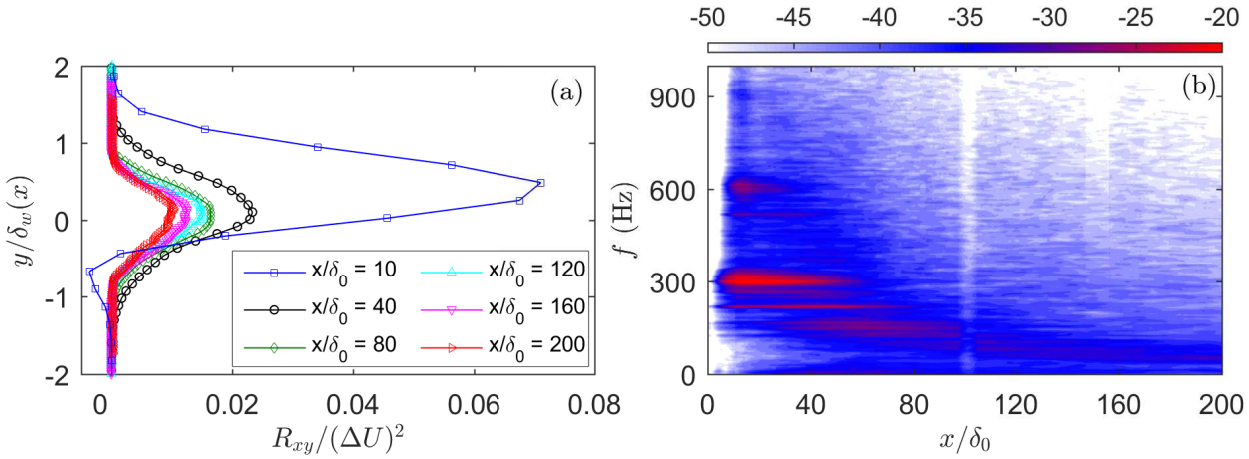

Fig. 5 (a) Profiles of Reynold's shear stress ($R_{xy} = -\overline{u'v'}$) at different streamwise locations non-dimensionalised with $(\Delta U)^2$. (b) Non-dimensional, normalised power spectra ($\Phi_N^{v'} \cdot \Delta f/(\Delta U)^2$ (dB), $\Delta f = 5$ Hz) of the v'-velocity component sampled along the $y_{0.5}$- line in figure 4a.

where Φ is the power spectral density (PSD) and ES is the temporal ensemble size. The summations are performed with respect to the corresponding subscript. The power spectra are non-dimensionalised with $(\Delta U)^2$.

The computed power spectra is shown in figure 5b. A discontinuity is observed in the power spectra at $x/\delta_0 \approx 100$ which is an artefact of the stitching of the near and far-wake PIV FOVs. A similar discontinuity is observed at higher frequencies close to $x/\delta_0 = 150$ which is expected to be due to the stitching of the frames of the two cameras when capturing the far-wake field done on *Davis*. The fluctuations with highest energy correspond to the frequencies in a band close to 300 Hz (±10 Hz) and are observed to be strongest close to the splitter plate. Thus, the fundamental KH instability in the current flow configuration is expected to have a frequency $f_0 = 300$ Hz. The energy of this frequency band reduces downstream and becomes comparatively low for $x/\delta_0 > 60$. Fluctuations at the harmonic of the fundamental frequency band ($f = 2 \cdot f_0 = 600$ Hz) are also observed. However they contain lesser energy and occur in a smaller region along the streamwise direction.

Fluctuations are also observed close to the frequency $f = 150$ Hz which is in the frequency band close to the first sub-harmonic ($f_0/2$) of the fundamental KH instability. The onset of these fluctuations are downstream compared to the fundamental instability as expected. Additionally they become strongest at $x/\delta_0 \approx 60$ which is approximately the location where the fluctuations of the fundamental instability are observed to become very weak. Fluctuations with a frequency $f = 220$ Hz are seen to co-exist with the fundamental instability although with less energy. However, the energy of these fluctuations maximise further downstream at $x/\delta_0 \approx 33$.

IV. Primary instability forcing

The instability modes that will be forced by the DBD plasma actuator with the low-frequency (f_b) square-wave burst modulation are chosen based on the observations of the the power spectra computed on the unforced mixing layer (figure 5b). Therefore, EFD forcing was applied to impart perturbations at the frequency of the fundamental Kelvin-Helmholtz instability $f_b = f_0 = 300$ Hz and its first sub-harmonic, $f_b = f_0/2 = 150$ Hz. The effect of this spanwise-uniform EFD forcing on the mixing layer is discussed here.

In the two cases presented here, the DBD plasma actuator is operated at voltage amplitude $V_{ac} = 14$ kV and AC frequency $f_{ac} = 2$ kHz. The AC frequency is responsible for the ionisation process and hence the production of the EFD force while the aforementioned burst modulation frequency excites the necessary instabilities in the mixing layer. The duty-cycle of the burst modulation is also held constant at 50%. To give an estimate of the performance of the DBD plasma actuators utilized here, at these operating conditions (voltage amplitude and AC frequency), the electric power consumption of the DBD actuator was measured to be approximately 0.6 W cm^{-1}. For this electric power, the maximum velocity in the jet induced by the DBD actuator is estimated to be approximately 4 m s^{-1} from [22] who reported the maximum induced velocity at different input electric power for a DBD actuator with a 2 mm thick PMMA plate as the dielectric substrate. The values of the average performance parameters is halved due to the burst modulation with 50%

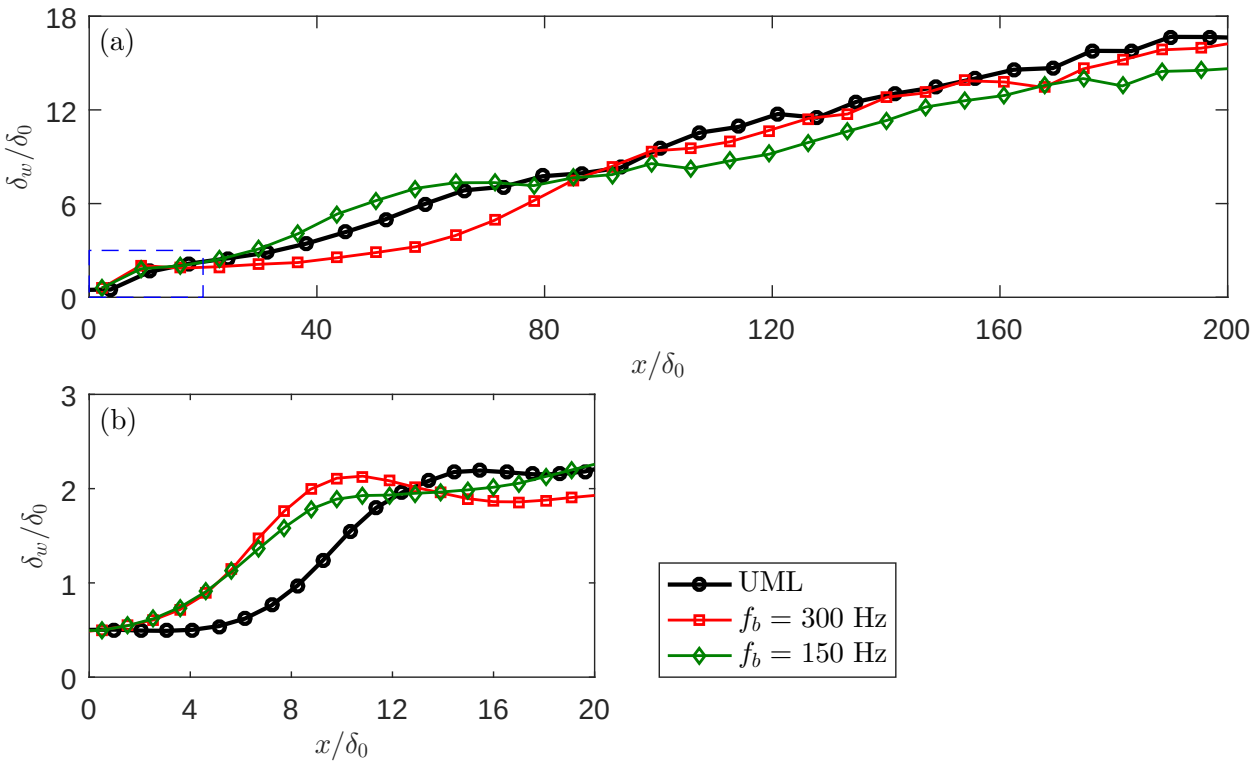

Fig. 6 (a) Vorticity thickness of the forced mixing layer. (b) Zoomed-in view of mixing layer growth in the dashed (blue) rectangle in (a).

duty cycle being applied. Thus, the power consumed by the current DBD actuator while applying the necessary control on the mixing layer is about 0.3 W cm^{-1} and the corresponding average velocity in the induced jet is approximated to be of the order of 2 m s^{-1} while the peak velocity is expected to be maintained still at 4 m s^{-1}.

The evolution of the vorticity thickness (equation 2) along the streamwise direction for the different forced mixing layers is presented in figure 6. The EFD forcing results in an initial development of the mixing layer occurring upstream compared to the unforced case as observed in the the zoomed-in view of the vorticity thickness close to the splitter-plate trailing edge (dashed (blue) rectangle in figure 6a) shown in figure 6b. Regardless of the forced instability mode, the initial development of the forced mixing layer is at $x/\delta_0 \approx 3$. This may be attributed to the action of the time-averaged momentum input by the DBD actuator against the splitter-plate wake.

It is shown in [21] that the effect of the splitter-plate wake strength reduces with the velocity ratio r of the mixing layer. In the current scenario, the applied EFD forcing accelerates the flow in the high-velocity boundary layer. This will result in a local reduction of the velocity ratio just downstream of the splitter-plate which ultimately leads to the reduction of the strength of the splitter plate wake. To give an estimate of the local change of velocity ratio, using the velocity estimated (2 m s^{-1}) in the jet induced by the DBD actuator mentioned earlier, the velocity of the high-velocity stream can be approximated to be 12 m s^{-1}. Thus, just downstream of the splitter-plate trailing edge, the velocity ratio will be $r \approx 0.42$ instead of $r = 0.5$ in the unforced mixing layer resulting in the weakening of the splitter-plate wake.

The initial growth of the forced mixing layer lasts until $x/\delta_0 \approx 9$. Further downstream, forcing the two different instabilities results in different growth patterns of the ensuing mixing layers as observed in figure 6a. Forcing the fundamental instability results in a interruption of mixing layer growth until $x/\delta_0 = 40$. This is expected to be due to the attenuation of sub-harmonic instabilities which play a pivotal role in mixing layer growth. The mixing layer then starts to grow, eventually collapsing on to the growth curve of the unforced mixing layer.

Application of forcing at the first sub-harmonic of the fundamental instability ($f_b = f_0/2 = 150$ Hz) leads to a different growth curve. After the sharp initial growth, the mixing layer grows linearly with a growth rate higher than the unforced mixing layer ($\approx 0.42 \cdot \lambda$). Post this, the growth halts temporarily from $x/\delta_0 = 60$ to about 110. The growth of this mixing layer is re-initiated downstream and it grows linearly thereafter until the end of the measured spatial domain at the same rate as the unforced mixing layer. When the growth curves of the two forced mixing layers are compared

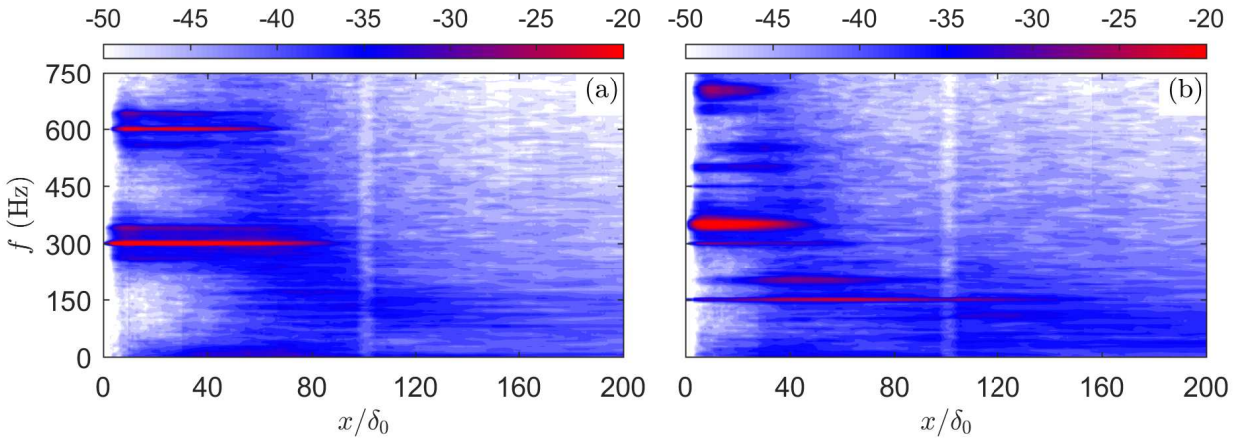

Fig. 7 Non-dimensional, normalised power spectra ($\Phi_N^{v'} \cdot \Delta f/(\Delta U)^2$ (dB), $\Delta f = 5$ Hz) of the v'-velocity component sampled along the $y_{0.5}$ line of the mixing layers forced at (a) $f_b = f_0 = 300$ Hz and (b) $f_b = f_0/2 = 150$ Hz.

with each other, it is observed that the streamwise location where the applied forcing has a significant influence varies. The effect of the fundamental KH instability forcing on the growth of the mixing layer is detected further upstream compared to when the sub-harmonic is forced. This is expected to be a consequence of the stability characteristics of the flow field as different perturbations are most amplified at different streamwise locations [3, 5].

As done on the unforced mixing layer (figure 5b), the normalised power spectra of fluctuations of the transverse velocity component (v'), sampled along the $y_{o.5}$ line of the two forced mixing layers is presented in figure 7. The power spectra of the mixing layer forced at the fundamental KH instability (figure 7a) shows significant fluctuations at the forced frequency $f_b = f_0 = 300$ Hz. These appear just downstream of the splitter-plate trailing edge and span until about $x/\delta_0 \approx 80$. This is further downstream compared to the unforced mixing layer where fluctuations of the fundamental KH instability frequency band were very low after $x/\delta_0 = 60$. Furthermore, the energy of fluctuations only at the forced instability is observed to be high here, unlike the unforced mixing layer where frequencies in a band around the fundamental instability were seen to contain high energy. Strong fluctuations are also observed at the harmonic of the forced fundamental instability. However, the energy in the frequency band of the sub-harmonic instabilities on the other hand are significantly reduced compared to the power spectra of the unforced mixing layer until $x/\delta_0 \approx 40$. This clearly shows the attenuation of sub-harmonic instabilities when the forcing is applied on the mixing layer at the fundamental instability.

When the mixing layer is forced at $f_b = f_0/2 = 150$ Hz, fluctuations at the forced sub-harmonic instability is observed in the power spectra (figure 7b). The energy of these fluctuations are seen just downstream of the splitter-plate trailing edge. The energy increases further downstream, reaching its maximum value at $x/\delta_0 \approx 60$. Beyond this location, a reduction in the energy is observed and after $x/\delta_0 = 120$ these fluctuations become very weak. Fluctuations at the frequency of the fundamental instability (which is the harmonic of the forced instability) is also observed, although weak, to last until about $x/\delta_0 \approx 40$. Strong fluctuations are also observed in the frequency band centred around 350 Hz, starting just downstream of the splitter-plate trailing edge and lasting until $x/\delta_0 \approx 40$. These fluctuations are expected to be the result of non-linear interaction of the forced instability mode with other instabilities naturally occurring in the mixing layer. However, no conclusive evidence of such a phenomenon can be discerned without further analysis.

The effect of the applied EFD forcing on the coherent vortices in the forced mixing layer, and the investigation of their dynamics and interactions due to the applied forcing is desired. As discussed in section II.C, the PIV acquisition was synchronized with the burst-modulation cycle. Thus, the phase-average of the instantaneous PIV time-series was computed at eight different phases separated by 0.25π of the low-frequency burst modulation. The Q-criterion, which is the second invariant of the velocity field [23], is computed to detect the coherent vortices in the mixing layer and observe their dynamics and interaction along one burst-modulation cycle. These results for the two forced mixing layers are presented in figure 8 and 9. The Q-criterion is non-dimensionalised with the maximum value (Q_{max}) in the corresponding field.

The Q-criterion of the phase-averaged velocity at five different phases along the burst-modulation cycle of the mixing

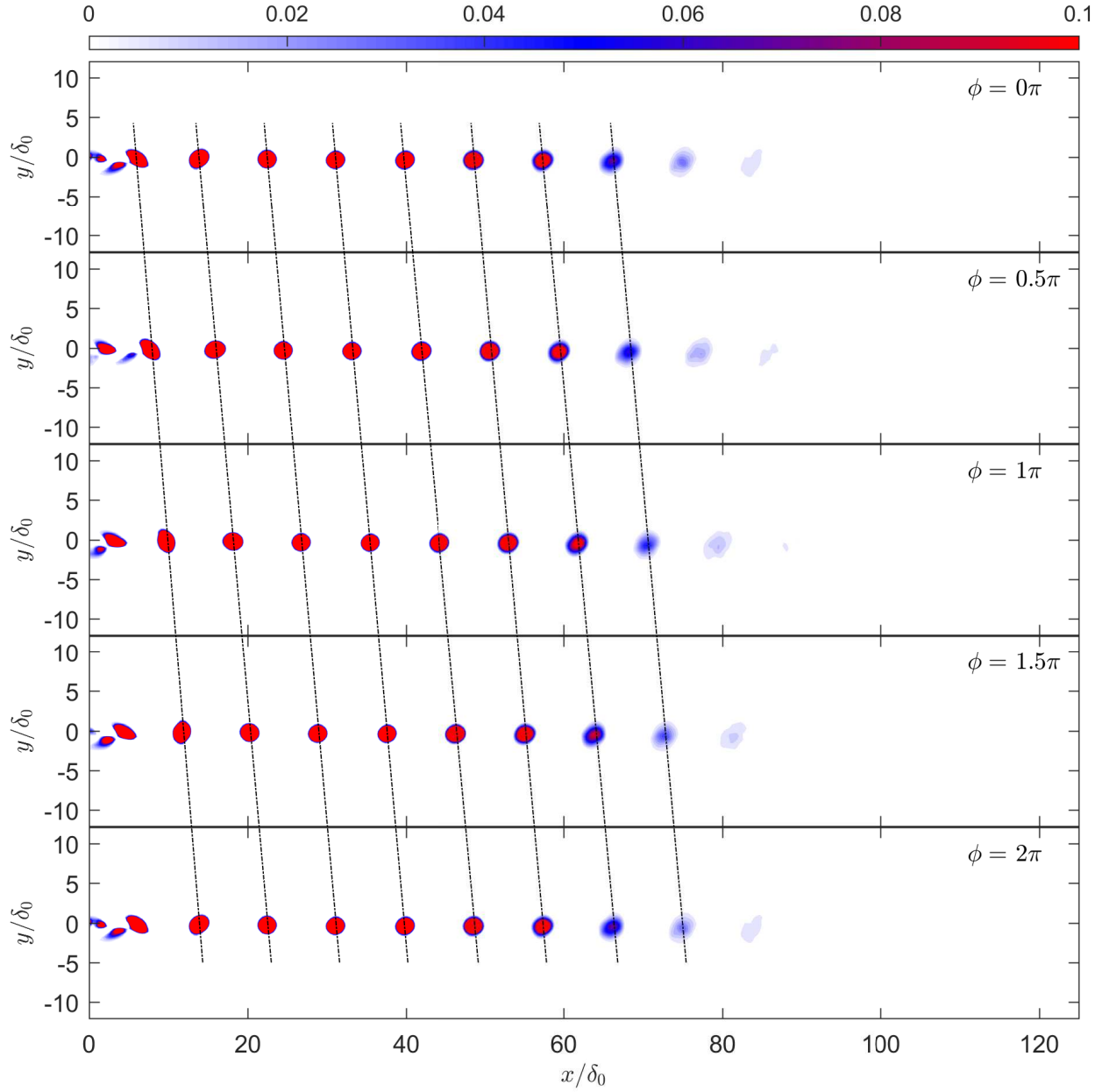

Fig. 8 Non-dimensional Q-criterion (Q/Q_{max}) computed on the phase-averaged velocity fields of the mixing layers forced at $f_b = f_0 = 300$ Hz at five different phases along the low-frequency burst modulation.

layer forced at the frequency of the fundamental KH instability is shown in figure 8. The applied EFD forcing results in amplification of the corresponding two-dimensional primary KH instability wave which rolls-up into the coherent vortices just downstream of the splitter-plate trailing edge as observed. The convection velocity of these coherent vortices is equal to the expected value of $\overline{U} = 7.5$ m s^{-1} [2, 3, 14] after the initial roll-up of vortices is complete.

In this forced mixing layer, no instance of vortex pairing is observed along the burst-modulation cycle. This is expected to be due to the attenuation of the sub-harmonic instabilities by the applied fundamental instability forcing as seen in the power spectra (figure 7a). Low energy of sub-harmonic instabilities compared to the fundamental instability was shown to inhibit vortex pairing in previous works [2, 7]. The strength of the coherent vortices seem to diminish along the streamwise direction and there are no clear coherent vortices noticeable after $x/\delta_0 = 80$. Thus, the current forced mixing layer is not in phase with the burst frequency of the applied EFD forcing any more. This streamwise

location is close to that where the growth of the current mixing layer became very similar to that of the unforced mixing layer as observed in figure 6a. This further supports the idea that this re-initiation of the growth must be a consequence of the natural amplification of sub-harmonic instabilities.

The non-dimensionalised Q-criterion computed on the phase-averaged velocity fields of the mixing layer forced at the first sub-harmonic of the fundamental KH instability are presented in figure 9. One instance of vortex pairing involving two vortices (dashed red rectangle in the field at phase $\phi = 0$) is observed in the current mixing layer. The interaction of these vortices along the burst modulation cycle is depicted in the snapshots presented in figure 10. The interaction of the forced sub-harmonic instability with the perturbations corresponding to the fundamental KH instability seems to result in the roll-up of vortices alternately close to and farther from their neighbours. The two vortices that are close to each other are observed to undergo pairing due to mutual induction as described in [7].

The vortex pairing process begins at $x/\delta_0 \approx 20$ and is completed at $x/\delta_0 \approx 50$ within two cycles of the burst modulation. The coherent vortices show no interaction after the completion of the vortex pairing which explains the temporary halt in the growth of the current mixing layer observed in figure 6a. After the pairing, the vortices convect downstream at a velocity of about 8 m s^{-1} which is comparable to the expected value. Here too, the vortices become weaker and eventually disappear after $x/\delta_0 \approx 110$. The linear growth of the mixing layer after $x/\delta_0 = 110$ is mainly attributed to the natural onset of other instabilities with frequencies lower than the forced sub-harmonic instability.

V. Concluding remarks

The influence of EFD forcing applied by a DBD plasma actuator on the coherent vortices in a turbulent mixing layer is investigated experimentally in this work. The effect of imparting fluctuations pertaining to the fundamental Kelvin-Helmholtz instability in the mixing layer and its first sub-harmonic on the growth of the mixing layer and the interaction of the vortices within, is studied here.

Amplification of the fundamental Kelvin-Helmholtz instability results in the inhibition of vortex pairing and consequently a local negligible growth of the ensuing mixing layer. This is expected to be due to the attenuation of sub-harmonic instabilities which is necessary for the occurrence of vortex pairing [5–7]. Imparting fluctuations at the first sub-harmonic of the fundamental instability, as expected, results in one instance of vortex pairing. The growth rate of the mixing layer is observed to be higher than the unforced case, in the streamwise extent where the vortex pairing process occurs, and stagnates thereafter. In both forced cases, the mixing layer eventually acquires a growth rate similar to that of the unforced mixing layer.

The results demonstrate that the applied EFD forcing, specifically the low-frequency burst modulation has a significant effect on the generation of spanwise vortices, their subsequent pairing and as a consequence the growth of the mixing layer. Performing linear stability analysis on the current flow field will shed more light on the the effect of different instability modes on stability of the flow. Additionally, to gain more insight into the effect of this unsteady low-frequency forcing, the spatial organisation of these fluctuating fields is also sought and can be obtained by applying proper orthogonal decomposition on the acquired PIV fields. These analytical tools will elucidate the interaction of the different instability waves in the mixing layer and aide in understanding the underlying phenomenon which causes the observed vortex dynamics better. Further research is also necessary to investigate the influence of the operating parameters of the DBD actuator on the mixing layer, in order to better design control strategies in the future.

Acknowledgments

This research is funded by the French Government program *Investissements d'Avenir* (LABEX INTERACTIFS, reference ANR-11-LABX-0017-01).

References

[1] Brown, G., and Roshko, A., "On density effects and large structure in turbulent mixing layers," *Journal of Fluid Mechanics*, Vol. 64, No. 4, 1974, pp. 775–816.

[2] Oster, D., and Wygnanski, I., "The forced mixing layer between parallel streams," *Journal of Fluid Mechanics*, Vol. 123, 1982, pp. 91–130.

[3] Ho, C., and Huerre, P., "Perturbed free shear layers," *Annual Review of Fluid Mechanics*, Vol. 16, No. 1, 1984, pp. 365–422.

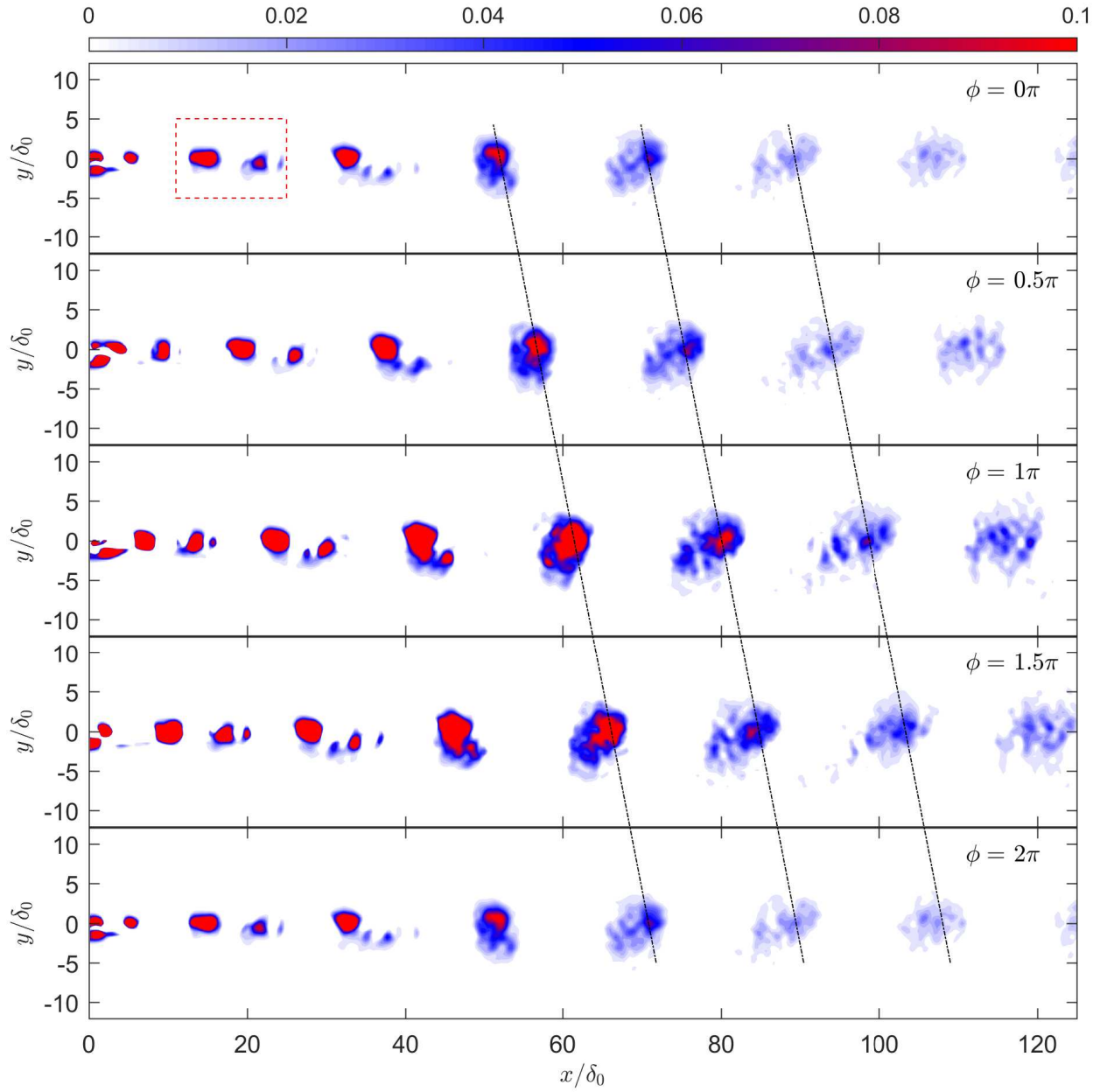

Fig. 9 Non-dimensional Q-criterion (Q/Q_{max}) computed on the phase-averaged velocity of the mixing layers forced at $f_b = f_0/2 = 150$ Hz at five different phases along the low-frequency burst modulation cycle.

[4] Winant, C., and Browand, F., "Vortex pairing: the mechanism of turbulent mixing-layer growth at moderate Reynolds number," *Journal of Fluid Mechanics*, Vol. 63, No. 2, 1974, pp. 237–255.

[5] Ho, C., and Huang, L., "Subharmonics and vortex merging in mixing layers," *Journal of Fluid Mechanics*, Vol. 119, 1982, pp. 443–473.

[6] Mansour, N., Hussain, F., and Buell, J., "Subharmonic resonance in a mixing layer," 1988, pp. 57–68.

[7] Husain, H., and Hussain, F., "Experiments on subharmonic resonance in a shear layer," *Journal of Fluid Mechanics*, Vol. 304, 1995, pp. 343–372.

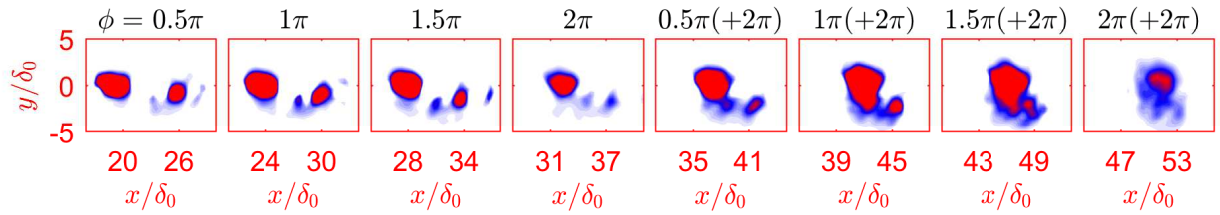

Fig. 10 Snapshots of the vortex pairing observed n the mixing layer forced at $f_b = f_0/2 = 150$ Hz (vortices in dashed red rectangle in the field at phase $\phi = 0$ in figure 9) along the low-frequency burst modulation cycle.

[8] Benard, N., and Moreau, E., "Electrical and mechanical characteristics of surface AC dielectric barrier discharge plasma actuators applied to airflow control," *Experiments in Fluids*, Vol. 55, No. 11, 2014, pp. 1–43.

[9] Grundmann, S., and Tropea, C., "Active cancellation of artificially introduced Tollmien–Schlichting waves using plasma actuators," *Experiments in Fluids*, Vol. 44, No. 5, 2008, pp. 795–806.

[10] Yadala, S., Hehner, M., Serpieri, J., Benard, N., Dörr, P., Kloker, M., and Kotsonis, M., "Experimental control of swept-wing transition through base-flow modification by plasma actuators," *Journal of Fluid Mechanics*, Vol. 844, 2018.

[11] Corke, T., and Thomas, F., "Active and Passive Turbulent Boundary-Layer Drag Reduction," *AIAA Journal*, 2018, pp. 1–13.

[12] Ely, R., and Little, J., "The Mixing Layer Perturbed by a Dielectric Barrier Discharge," *43rd AIAA Fluid Dynamics Conference*, 2013, p. 2753.

[13] Little, J., and Kaul, U., "Mixing Layer: Numerical and Experimental Control Strategies," *45th AIAA Fluid Dynamics Conference*, 2015, p. 3343.

[14] Oster, D., Wygnanski, I., and Fiedler, H., "Some preliminary observations on the effect of initial conditions on the structure of the two-dimensional turbulent mixing layer," *Turbulence in Internal Flows (ed. S.N.B. Murthy)*, 1977, pp. 67–87.

[15] Laizet, S., Lardeau, S., and Lamballais, E., "Direct numerical simulation of a mixing layer downstream a thick splitter plate," *Physics of Fluids*, Vol. 22, No. 1, 2010, p. 015104.

[16] Huang, L., and Ho, C., "Small-scale transition in a plane mixing layer," *Journal of Fluid Mechanics*, Vol. 210, 1990, pp. 475–500.

[17] Abramovich, G., "The theory of turbulent jets," 1963.

[18] Sabin, C., "An analytical and experimental study of the plane, incompressible, turbulent free-shear layer with arbitrary velocity ratio and pressure gradient," *Journal of Basic Engineering*, Vol. 87, No. 2, 1965, pp. 421–428.

[19] Braud, C., Heitz, D., Arroyo, G., Perret, L., Delville, J., and Bonnet, J., "Low-dimensional analysis, using POD, for two mixing layer–wake interactions," *International Journal of Heat and Fluid Flow*, Vol. 25, No. 3, 2004, pp. 351–363.

[20] Bell, J., and Mehta, R., "Development of a two-stream mixing layer from tripped and untripped boundary layers," *AIAA journal*, Vol. 28, No. 12, 1990, pp. 2034–2042.

[21] Mehta, R., "Effect of velocity ratio on plane mixing layer development: Influence of the splitter plate wake," *Experiments in Fluids*, Vol. 10, No. 4, 1991, pp. 194–204.

[22] Jolibois, J., and Moreau, E., "Enhancement of the electromechanical performances of a single dielectric barrier discharge actuator," *IEEE Transactions on Dielectrics and Electrical Insulation*, Vol. 16, No. 3, 2009, pp. 758–767.

[23] Hunt, J., Wray, A., and Moin, P., "Eddies, streams, and convergence zones in turbulent flows," *Center for Turbulence Research Report CTR-S88*, 1988, p. 193–208.